scientific reports

OPEN

Piezoelectric properties improvement in soft membrane with wet-spinning prepared barium titanate/polyvinylidenefluoride composites fiber

Xiong-Wei Lin[1,2✉], Prasad Gajula[2,3✉], Xiao-shan Luo[5], Mingrui Zhao[2], Xiao-bo Zhao[2] & Ye Fan[4✉]

Piezoelectric composite materials have demonstrated significant potential for developing high-performance wearable sensors. However, optimizing the piezoelectric output performance in polymer-based devices remains challenging due to the suboptimal synergy between the piezoelectric reinforcement phase and substrate materials. Moreover, the instability of response signals further hampers the sensor's practical utility. In this investigation, wet-spinning technology was applied to fabricate a novel Barium Titanate (BaTiO$_3$)/Polyvinylidene fluoride (PVDF) composite fiber. Through this approach, we enhanced the piezoelectric properties of the material. Notably, our electron diffraction analysis revealed compelling lattice deformations in the ceramic particle-polymer interface, yielding significant enhancements in the piezoelectric characteristics. Remarkably, incorporating just 1.5 wt% of BaTiO$_3$ in PVDF led to a piezoelectric output of 0.88 V during dynamic cycle tests at 1 Hz. Encouragingly, the output signal exhibited a robust linear correlation (R^2 = 0.996) with applied compression force.

Piezoelectric materials play a pivotal role in wearable sensors[1]. Drawing from the mechanism of pressure signal propagation, the utilization of polytetrafluoroethylene (PTFE) and fluorinated ethylene propylene (FEP) materials has come to the fore. These materials are integral to the construction of fluorocarbon piezoelectric pressure sensors (FPS)[2], a technology specifically designed to track radial artery pulse waves. Furthermore, the combination of PVDF and ZnO has proven valuable in gesture-based remote-control applications[3]. Notably, composites intertwining carbon nanotubes and polyvinylidene fluoride (CNT/PVDF) have been ingeniously designed as shoe sensors. These composite sensors exhibit the remarkable capability of not only performing assessments but also providing personalized guidance for football training[4]. Unlike non-polar carbon chains, PVDF demonstrates ferroelectricity due to its repeated -CH$_2$-CF$_2$- monomer units[5]. Moreover, the electropositive hydrogen atoms and electronegative fluorine atoms allow PVDF to form five crystalline phases: α, β, γ, δ, and ε[6]. Typical wearable piezoelectric sensors also include ceramic/polymer composites. Ceramic materials exhibit high piezoelectric constants but are limited by their rigidity[7]. In contrast, polymers generally offer greater flexibility[8] but are hindered by low piezoelectric voltage coefficients. Consequently, the development of flexible ceramic/polymer composites that combine the advantages of both ceramics and polymers has garnered significant attention in recent decades[9–11], aiming to achieve piezoelectric composites with excellent sensitivity.

[1]School of Microelectronics, Shenzhen Institute of Information Technology, Shenzhen 518000, China. [2]Guangdong Provincial Research Center on Smart Materials and Energy Conversion Devices, Guangdong Provincial Key Laboratory of Functional Soft Condensed Matter, School of Materials and Energy, Guangdong University of Technology, Guangzhou 510006, China. [3]Department of Advanced Materials Engineering for Information & Electronics, Kyung Hee University, Yongin 17104, Gyeonggi-do, South Korea. [4]Institute for Frontier Materials, Deakin University, 75 Pigdons Road, Waurn Ponds, VICMelbourne 3216, Australia. [5]School of Materials and Environmental Engineering, Shenzhen Polytechnic University, Shenzhen, China. ✉email: linxw_gdut_edu@126.com; gajula@khu.ac.kr; y.fan@deakin.edu.au

Recent research on PVDF has shown that the preparation of nanofiber mats by electrospinning is an effective method for producing the β phase in PVDF[12]. After electrospinning, PVDF predominantly exhibits a mix of α and β phases, and further doping with inorganic ceramic materials can enhance its piezoelectric and ferroelectric properties[13]. Common inorganic ceramic dopants include zinc oxide (ZnO)[14], lead zirconate titanate ($PbZr_{0.52}Ti_{0.48}O_3$, PZT)[15], and barium titanate ($BaTiO_3$, BT)[16]. Among these, $BaTiO_3$, as an environmentally friendly, lead-free piezoelectric material with a high piezoelectric strain coefficient, has received significant attention.

Nonetheless, incorporating $BaTiO_3$ as a piezoelectric reinforcing phase in nanocomposites presents challenges due to its weak interfacial bonding and inadequate dispersion. These issues significantly undermine the electromechanical properties of the nanocomposites, including stress/strain response and piezoelectric coefficients. As a result, the potential for enhancing piezoelectric output performance is severely limited[17]. Furthermore, due to the inherent porosity of the material, the device exhibits substantial changes in dipole moment during compression and release cycles. This tendency to generate imbalanced signal outputs while monitoring subtle signals undermines the composite fiber's viability for sensor applications[18]. In composite preparation, the conventional electrospinning process often induces excessive aggregation of filler particles within the polymer matrix[19]. The agglomeration of $BaTiO_3$ particles disrupts the piezoelectric dipole dynamics[20], while interface defects trap generated charges, leading to increased leakage current[21]. These combined effects hinder the enhancement of piezoelectric nanocomposite performance. Additionally, in conventional electrospinning processes that involve metal collectors, charges frequently dissipate through these collectors during spinning. This reduced retention of effective charges on the fibers adversely affects the high-pressure bonding at the organic-inorganic material interface[22]. As a result, the interaction between $BaTiO_3$ and PVDF in the $BaTiO_3$/PVDF (BT/PVDF) composite weakens, reducing the transmission of applied stress from the matrix to $BaTiO_3$. This ultimately leads to decreased mechanical conversion efficiency and a deterioration in composite performance. Therefore, numerous studies have emphasized the importance of optimizing the effective combination of the piezoelectric reinforcement phase with the base material. These studies suggest that such optimization is crucial for increasing the βphase content in PVDF, which enhances piezoelectric performance, and for significantly improving the application potential of composite fibers. For instance, Netzahualpille et al. introduced a bubble electrospinning setup where the electrode was integrated within the polymer solution reservoir[23]. Similarly, Greiner et al. manipulated membrane morphology by electrospinning poly(L-lactide) (PLLA) atop a liquid reservoir to promote polymer crystallization[24]. Kong et al. achieved a thin surface layer on nanofibers by increasing humidity during their experiment. This layer slowed solvent evaporation, delaying nanofiber solidification and providing sufficient time for β-phase nucleation and growth[25]. Zhang et al., on the other hand, enhanced the interaction between the polymer matrix and $BaTiO_3$ nanoparticles by incorporating graded methacrylate monomers (MMA or TFEMA) onto the surface of BT nanoparticles within the PVDF matrix[26]. Using the non-solvent-induced phase separation (NIPS) effect[27], they exploited the lack of hydrogen-bond interactions between PVDF interfaces and water[28]. This allowed low-conductivity water to function as a collector without disrupting the spinning process. Consequently, they achieved increased accumulation of electret charges within the composite, enhancing effective polarization at the organic-inorganic interface[29]. To date, various studies have reported on PVDF/$BaTiO_3$ composites to improve piezoelectric performance using techniques such as casting, spinning and electrospinning. However, the wet-electrospinning technique for PVDF-BT composites has not yet been explored.

This study comprehensively explores the crystallinity of BT/PVDF nanofibers in the context of a water collector and analyzes the influence of $BaTiO_3$ particles on the piezoelectric output characteristics of PVDF fibers. Flexible BT/PVDF piezoelectric composites were meticulously prepared, ensuring uniform fiber diameters and filler concentrations ranging from 0.5 to 1.5 wt%. While the literature on piezoelectric composites and electrospinning is extensive, our study offers a nuanced perspective by demonstrating that, at filler concentrations of 0.5–1.5 wt%, lattice distortion between BT and PVDF plays a more pivotal role in enhancing piezoelectric performance than merely increasing the β-phase content in PVDF. This effect is particularly pronounced when optimal compatibility is achieved through interface lattice distortion between the inorganic filler and the organic matrix. Moreover, our use of a water collector-assisted electrospinning technique further improved interfacial compatibility. Upon final packaging, the BT/PVDF composite exhibited an average piezoelectric output of 0.88 V under a 50 N compression force, with a highly linear correlation between the output and the applied force (R^2 = 0.996). These findings not only validate the key role of interface engineering in enhancing piezoelectric performance but also offer novel optimization strategies for sensor and related applications.

Methods and materials

Materials
PVDF powder with trade name Kynar 761 with an average molecular weight of 5.2×10^5 g/mol procured from Arkema, Guangzhou, China. Repolarization barium titanate (BT) powders were used in this study and procured from Qijin Materials, China, and Sinocera, China, respectively. The solvents N, N-dimethylformamide (DMF), and acetone were purchased from Damao Chemicals, Tianjin, China, and used without further purification. The metallic needle 19G with 0.68 mm inner diameter was purchased from Aladdin Reagent, China. The packaging material uses Kapton tape (50 μm) and copper foil as the electrode layer.

Methodology
Based on our previous reports on optimizing electrospinning conditions[32,33], here the PVDF film was prepared by dissolving 14 wt% PVDF powder in a solvent mixture of DMF and acetone (6/4) using magnetic stirring at 60 °C for 6 h and ultrasonic treatment for 30 min. Put the solution into a 20 mL syringe for electrospinning, and prepare the fibrous membrane vertically using the Lepton Technology electrospinning & spray unit (QNZT-E04)

and water collector. The electrospinning parameters are used for 20 kV high voltage, the flow rate is 1 mL h- 1, and the distance from the tip to the collector (aluminum foil) is 15 cm. In addition, the collector is immersed in 5 mm of water. Electrospinning is carried out under atmospheric conditions with a relative humidity of 75–85%. Before preparing the composite membrane, the ceramic particles were dispersed into an appropriate amount of anhydrous ethanol, subjected to high-energy ultrasonic treatment at 60 °C for 3 h, and dried at 120 °C for 2 h. After adding different weight% (0.5, 1.0, and 1.5) into the PVDF precursor solution, ultrasound was performed again for 20 min, and electrospinning was performed according to the same steps above. The complete schematic representation of preparation is explained in detail in Fig. 1(a). During the electrospinning process when the applied voltage overcame the surface tension, the solution became elongated and formed a Tylor cone beyond that the solution started to eject from the Tylor cone and started spinning the pictorial representation of the formation of the Tylor cone as shown in Fig. 1(b). Finally, PVDF and composite membrane were collected from water, dried in a hot air oven at 60 °C, and then further characterized. The detailed characterization techniques were discussed in Supporting Information section S1.

Results and discussion
Structural and crystal studies

The surface morphology of the as-received $BaTiO_3$ powder, electrospun PVDF, and BT/PVDF composites was analyzed using field emission scanning electron microscopy (FESEM), as shown in Fig. 2. Pristine PVDF fibers exhibited an irregularly arranged fibrous morphology with uneven fibers, primarily due to the use of a water medium during electrospinning[32]. Upon incorporating different amounts of BT, the resulting electrospun membranes displayed a mixture of fibers and BT particles (Fig. 2b-d). The as-received BT powder demonstrated a spherical morphology (Fig. 2e), and its combination with PVDF fibers indicated the successful formation of composite films. The effect of BT content on fiber diameter was analyzed using Image-J software. Fiber diameters were measured at over 40 locations, with average values provided in **Table S2** (Supporting Information). The fiber distribution plots are shown as insets in Fig. 2a-d, and the average fiber diameters for PVDF and BT/PVDF composites are summarized in Fig. 2f. Pristine PVDF fibers had an average diameter of 0.37 μm, which gradually increased to 0.6 μm with the addition of 1.5 wt% BT. This increase in fiber diameter can be attributed to the incorporation of BT powder, which raises the viscosity of the solution as BT content increases (see Supporting Information Section **S1** and **Table S3**). Generally, higher solution viscosity correlates directly with increased fiber diameter[34]. The regional distribution of BT aggregation, both before and after electrospinning, was also analyzed using Image-J software. Results, shown in **Table S7** and **Fig. S4** (Supporting Information), indicate that while the distribution of BT particles remains uniform, the particle size slightly increases to 0.5 ± 0.1 μm after agglomeration. This increase could result from possible agglomerations or the particles being surrounded by the PVDF polymer. Additionally, the spherical shapes of the BT particles were distorted during magnetic stirring and ultrasonication during solution processing. Smaller BT filler sizes have been reported to enhance piezoelectric performance by accommodating more interaction sites[35]. This suggests that controlling particle size and distribution is crucial for optimizing the material's piezoelectric properties.
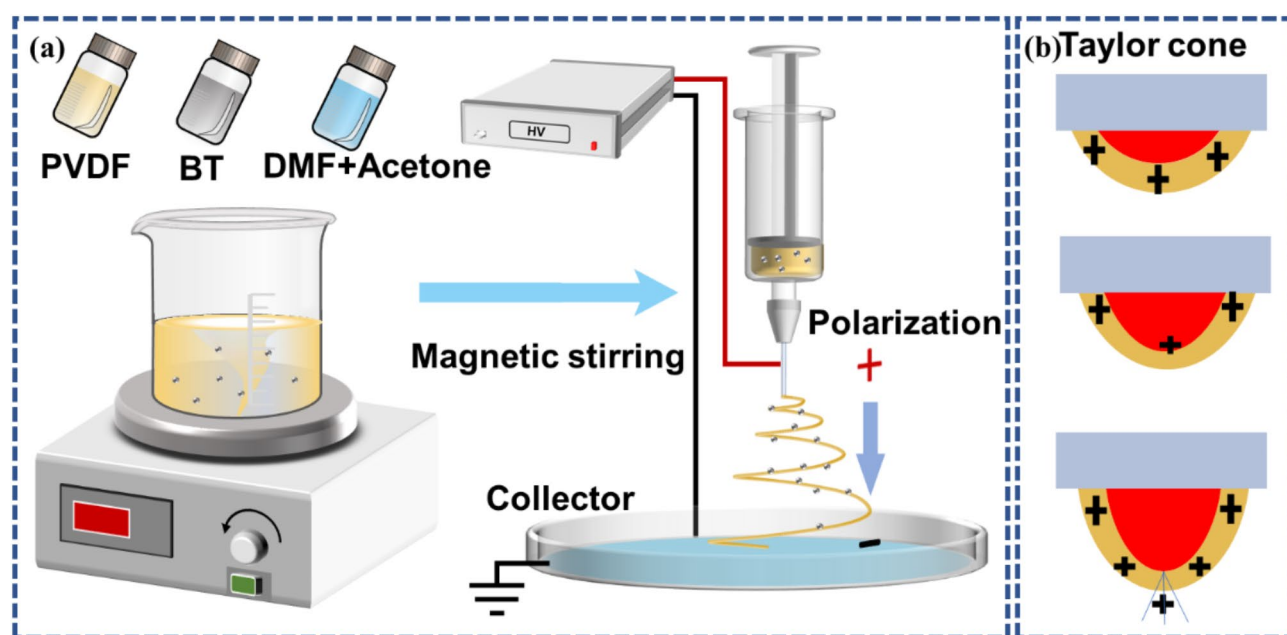

Fig. 1. (**a**) Schematic diagram of the principle of preparing piezoelectric composite fiber by wet electrospinning technology, (**b**) Schematic illustration of the formation of Taylor Cone-jet in electrospinning. Figure 1a and b were generated using Microsoft PowerPoint (Version 2019), available at https://www.microsoft.com.
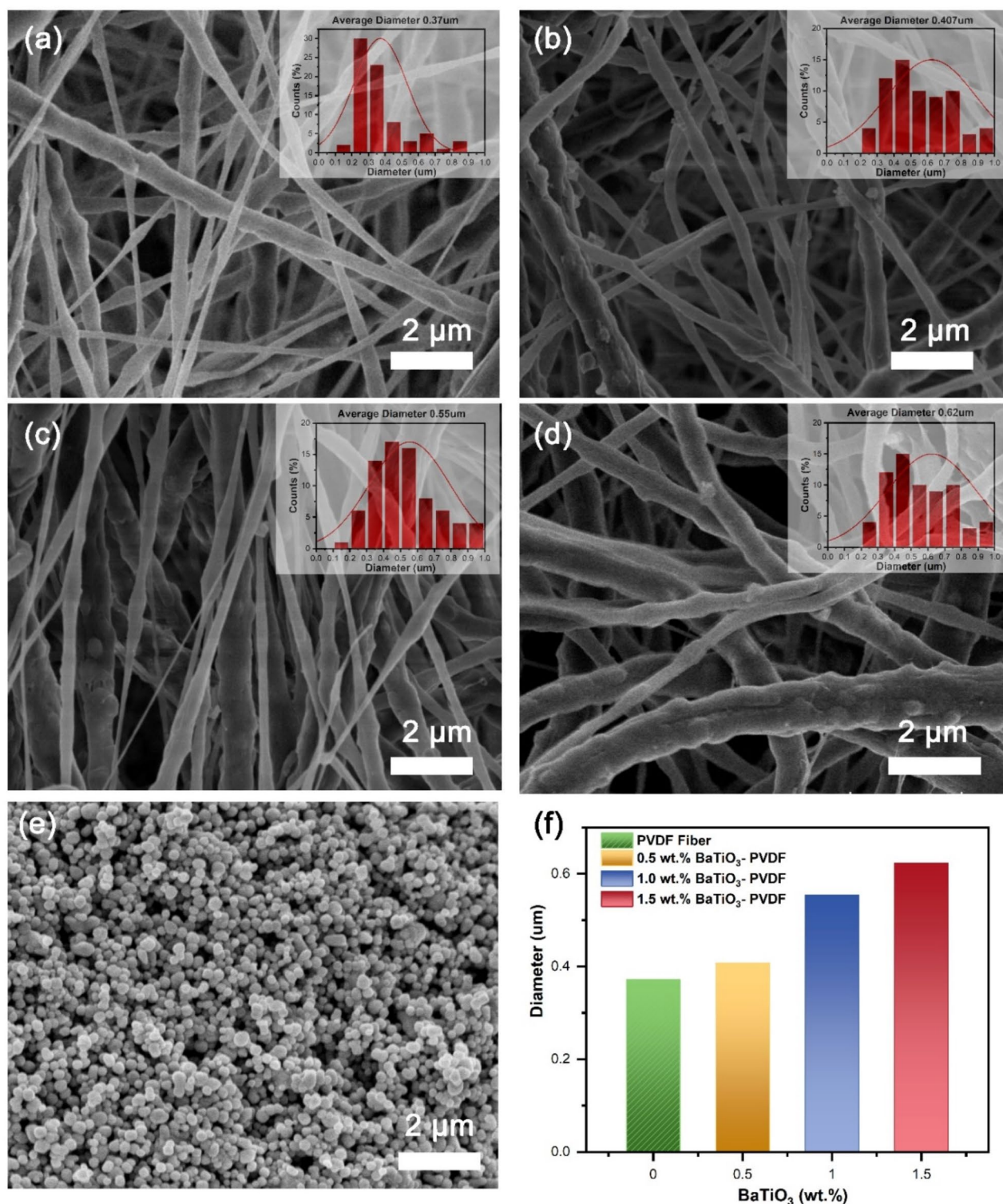
Fig. 2. Surface morphology of electrospun membranes (**a**) Pristine PVDF fibers, (**b**) 0.5 wt% BaTiO$_3$-PVDF fiber, (**c**) 1.0 wt% BaTiO$_3$-PVDF fiber, (d) 1.5 wt% BaTiO$_3$-PVDF fiber, (**e**) as-received BaTiO$_3$ powder, and (**f**) Distribution of fiber diameter for electrospun membranes as a function of BaTiO$_3$ content.

In the experiment, piezoelectric ceramic particles with low doping content (0.5–1.5 wt%) were selected to minimize the likelihood of filler particle agglomeration[30]. Under the established spinning conditions, the fiber diameter exhibited a uniform distribution, and the piezoelectric ceramic particles were well-integrated with the polymer fibers. The phase composition and purity of the composite fibers prepared by electrospinning were characterized using X-ray diffraction (XRD) (Fig. 3a). The pristine PVDF powder displayed primary 2θ peaks
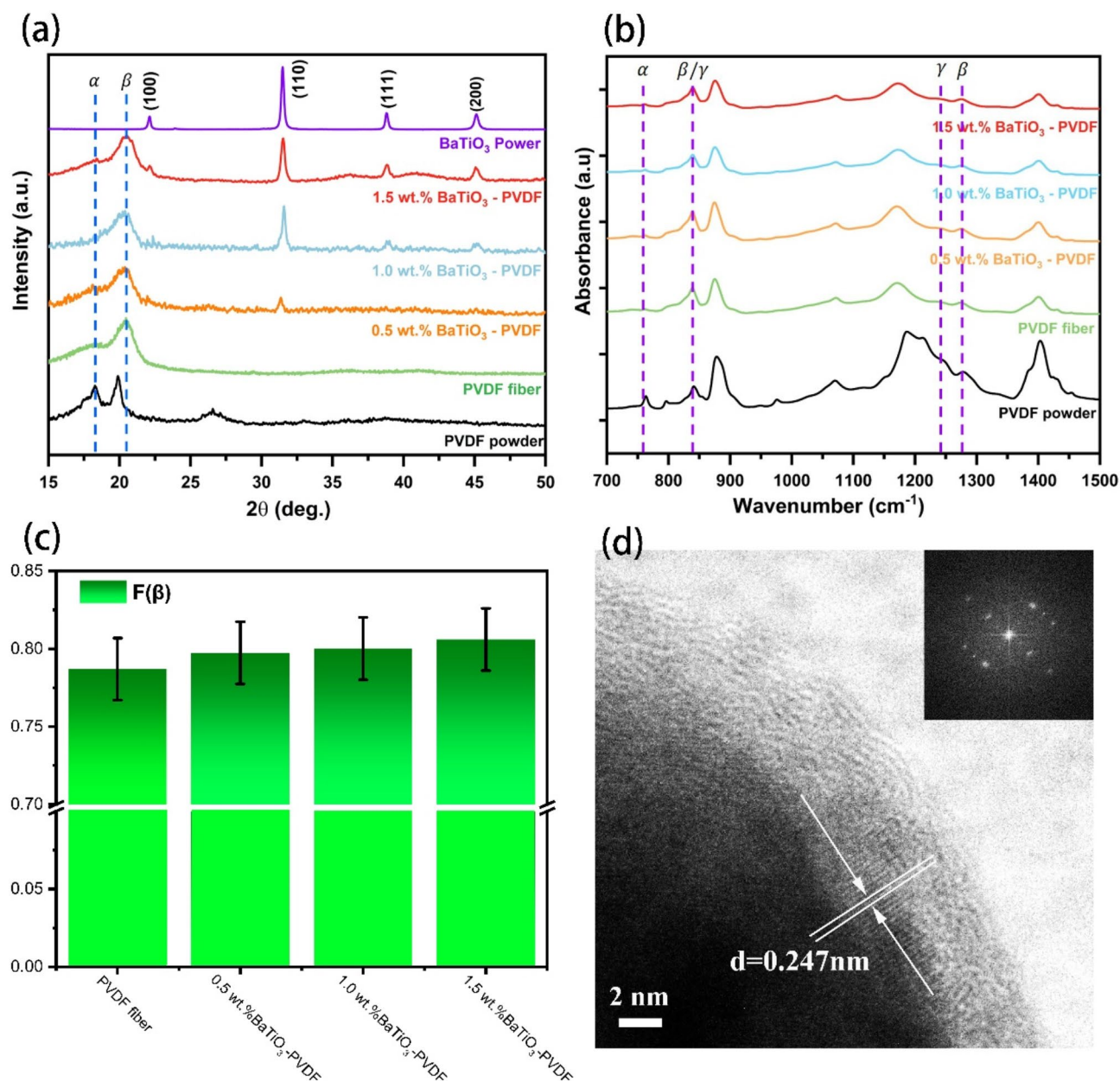
Fig. 3. (**a**) XRD patterns for as-received powders and electrospun samples, (**b**) FTIR-ATR spectra for as-received powders and electrospun samples, (**c**) content of crystalline β of BT/PVDF, (**d**) TEM image of 1.5 wt% BaTiO$_3$-PVDF.

at 18.2°, 19.9°, and 26.5°, corresponding to the α phase, attributed to the reflections of (110), (020), and (021) planes, respectively. In contrast, the PVDF and BT/PVDF composite fibers exhibited a single broad peak at 20.3° (for 0.5 and 1.0% BT) and 20.7° (for 1.5 wt% BT), replacing the three distinct α crystallization peaks shown in Fig. 3a. This broad peak is attributed to the α crystalline phase (020) and an overlapping contribution from unresolved β crystalline phases (110)/(200)[31]. Additionally, the XRD patterns of BT/PVDF fiber mats revealed the characteristic β phase peaks, alongside distinct BT ceramic peaks at 22.1° (100), 31.4° (110), 38.7° (111), and 45.07° (200) (PDF card 97 - 016- 6225).

To gain detailed information about the phase transitions in the samples, FTIR-ATR (Fourier-Transform Infrared Spectroscopy: Attenuated Total Reflectance) analysis has been used. Figure 3b shows the FTIR-ATR spectra of the untreated PVDF powder, pristine PVDF fiber, and BT/PVDF composite fiber. In each sample, the appearance of absorption bands at 763 cm^{-1} corresponding to the non-polar α phase in the FTIR spectrum. The exclusive peak at 1275 cm^{-1} corresponds to the β phase, while the peak at 1234 cm^{-1} indicates the presence of the γ phase. Intensive absorption band at 840 cm^{-1} is shared by both the β and γ phases[32,33].

The exact β phase percentage of the neat PVDF and its composite films were measured by Lamberts-Beer law as follows. The overall percentage of the β phase was calculated from Eqs. (1)-(2) based on the Lambert-Beer law[34].

$$F_{EA} = \frac{I_{EA}}{\left(\frac{K_{EA}}{K_\alpha}\right) I_\alpha + I_{EA}} \times 100\% \tag{1}$$

where I_{EA} and $I_\propto$ are the absorbance at 840 and 763 cm^{-1}, respectively, and K_{EA} and $K_\propto$ represent the absorption coefficients at the corresponding wavenumbers, which are 6.1 × 10^4 and 7.7 × 10^4 cm^2 mol$^{[-1}$, respectively. The relative fraction of β phases can also be calculated by Eq. (2), respectively.

$$F(\beta) = F_{EA} \times \frac{\Delta H_\beta}{\Delta H_\beta + \Delta H_\gamma} \tag{2}$$

ΔH_β is the absorbance difference between the peak around 1275 cm^{-1} and the nearest valley around 1260 cm^{-1} and ΔH_γ is the height difference between the peak around 1234 cm^{-1} and the nearest valley around 1225 cm^{-1}. The calculated β phase percentage is provided in Fig. 3c and Table S6.

Based on the calculation results, the addition of BT leads to a slight increase in the β phase in PVDF, with no significant further increase observed as the BT content is raised. Further investigate the interface interaction of piezoelectricity through TEM. The FE-TEM image of locally magnified 1.5 wt% BT/PVDF nanofiber is displayed. Figure 3d and **Fig. S5** (Supporting Information) show the TEM morphology of embedded BaTiO$_3$ in the boundary of the PVDF fiber surface at 1.5 wt%. According to TEM images and electron diffraction patterns, the spacing of the lattice plane in Fig. 3d is 0.247 nm, which changes 6 to 38% from the primary lattice spacing of (100) (110) (200) (PDF # 97 - 016- 6225). The change of surface spacing leads to lattice change. This enhanced lattice distortion is equivalent to a substantial electric dipole, which increases the polarization vector on the surface of BaTiO$_3$ crystal, and the absorbed free electrons transfer rapidly under the influence of the particle electric field, which improves the intrinsic piezoelectric effect[35].

Electrical characterization

The complete schematic diagram of the device is shown in Fig. 4a. Preparation of the piezoelectric sensing device: The BT/PVDF fiber mat has a thickness of approximately 100 µm and is covered on both sides with copper foil and a 50 µm Kapton tape. The overall dimensions of the device are 1.5 × 1.5 cm². The testing samples for piezoelectric output performance are subjected to reciprocating force via a grounded aluminum plate. Structurally, the samples consist of a Kapton shielding layer, a front electrode, the composite fiber membrane,
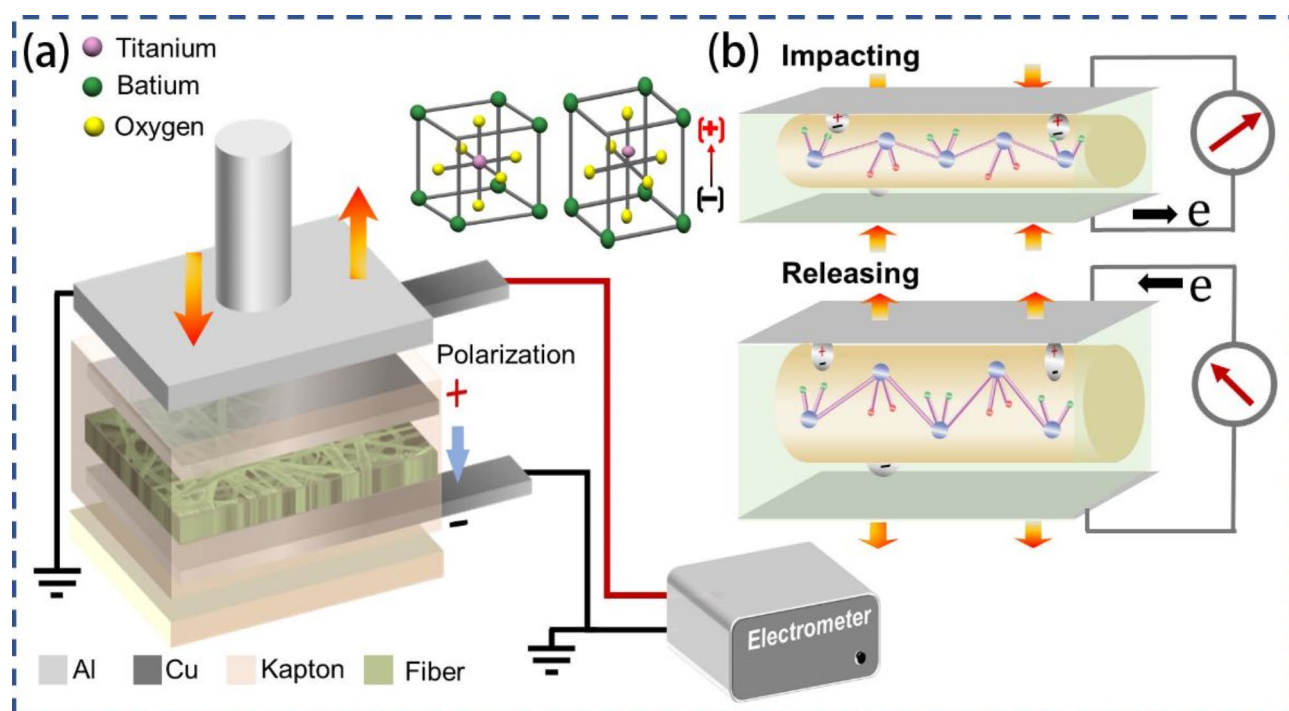
Fig. 4. (**a**) Illustrates the crossectional view of the piezoelectric device, (**b**) working mechanism of piezoelectric device. Figure 4a and b were generated using Microsoft PowerPoint (Version 2019), available at https://www.microsoft.com.

and a rear electrode. The complete schematic representation of the cross-sectional view of the device is shown in Fig. 4a.

The finite deformation of the piezoelectric fiber leads to smaller displacements, which allow the piezoelectric signal to reach its peak more quickly. The piezoelectric signal is primarily force-dependent, so the electric force relationship is tested accordingly. Figure 4b shows the electrical generation characteristics of the BT/PVDF nanofiber during pressing and releasing cycles. In the initial unpressurized state, the cations and anions' charge centers are aligned, with no significant polarization. Upon pressure application, the deformation of the fibers generates negative strain and reduces the volume. The separation of charge centers forms electric dipoles, which leads to the development of a piezoelectric potential between the electrodes. If the electrodes are connected to an external load, the piezoelectric effect drives electrons through the external circuit, partially screening the piezoelectric potential and reaching a new equilibrium state. This process converts mechanical energy into electrical energy, consistent with the principles of nanoelectronics[36].

The piezoelectric effect of the composite fibers is primarily attributed to the intrinsic contribution, which arises from field-induced lattice distortion[37]. Under the influence of lattice stress or polarization vector rotation[38], changes in the lattice parameters lead to lattice deformation. For the BT/PVDF composite, $BaTiO_3$ particles are uniformly distributed within the organic matrix. When an electric field is applied, the different polarization abilities of the ceramic particles and the polymer matrix generate bound charges at the BT/PVDF interface, causing local electric field distortion. Inorganic ceramic particles, like $BaTiO_3$, exhibit stronger polarization, leading to more significant bound charges on their surfaces. The composite's internal electric field is the sum of the applied and bound electric fields, which enhances the formation of intrinsic piezoelectricity under field-induced lattice distortion.

Due to the weak conductivity of wet spinning technology, the spinning process tends to increase the bound charge, which indirectly improves the piezoelectric properties of the composite fibers. During the spinning process, PVDF undergoes a phase transition to form β chains (trans chains). Adding BT particles can slow down this relaxation[39], and the slowing effect is due to the interface interaction[34] (characterized by TEM, **Fig. S5**, and Fig. 3d). However, excessive agglomeration and uneven distribution of BT particles can lead to output nonlinearity. Therefore, the wet spinning method is used to control the degree of BT agglomeration, preventing a decrease in interface charge density. The results from this study show that increasing the BT content improves the linearity and stability of the output voltage, confirming that the composite fibers are well-suited for sensor applications.

Figure 5a shows the output force and open-circuit voltage (V_{OC}) of PVDF and BT/PVDF composite membranes with varying BT content. The pristine PVDF fibers membrane exhibits a V_{OC} of 0.3 V. The V_{OC} increases gradually from 0.3 V to 0.88 V as the BT content increases from 0 wt% to 1.5 wt%. The piezoelectric performance of the optimized 1.5 wt% BT/PVDF device was evaluated as a function of frequency and load, as shown in Fig. 5b. Meanwhile, the d33 value was measured, and the results show that it increased exponentially with increasing BT content (Fig. 5c). However, this increase in d33 value did not directly correspond to a proportional increase in the output electrical performance. This is because the binding sites between BT powder and fibers are fixed, and the degree of dispersion remains relatively consistent in the range of 0.5–1.5 wt% BT. However, as the BT content increases, agglomeration can occur, limiting further improvements in piezoelectric properties due to reduced interfacial interactions, as shown in **Fig. S5**. When the frequency varied from 0.5 to 2.0 Hz in intervals of 0.5 Hz, the VOC remained relatively stable when the applied load was fixed at 50 N. Therefore, we conclude that the V_{OC} of the 1.5 wt% BT/PVDF device is independent of frequency. Additionally, as the applied load increased from 5 N to 50 N, the VOC of the 1.5 wt% BT/PVDF device increased from 0.1 V to 0.88 V, demonstrating good linearity ($R^2 = 0.996$) in this range (Fig. 5d). The presence of $BaTiO_3$ particles in the composite leads to the formation of stress concentration points within the fiber. When force is applied at these points, the localized stress increases, enhancing the output voltage[40].

Conclusion

In conclusion, this study successfully employed the wet electrospinning process to craft BT/PVDF composite fibers, which demonstrate enhanced sensing capabilities. Our analysis revealed that the wet spinning process not only retains the advantages of traditional techniques for β phase enhancement but also significantly improves interface interactions between the organic and inorganic components. This enhancement further augments the piezoelectric performance of the materials. Notably, the BT/PVDF composite containing 1.5 wt% BT exhibited a remarkable peak piezoelectric voltage of 0.88 V under a 50 N compression force, representing a 3-fold increase compared to unfilled PVDF fibers. This method, as an environmentally conscious approach to composite manufacturing, holds significant promise for the production of large-scale, cost-effective medical and wearable systems.
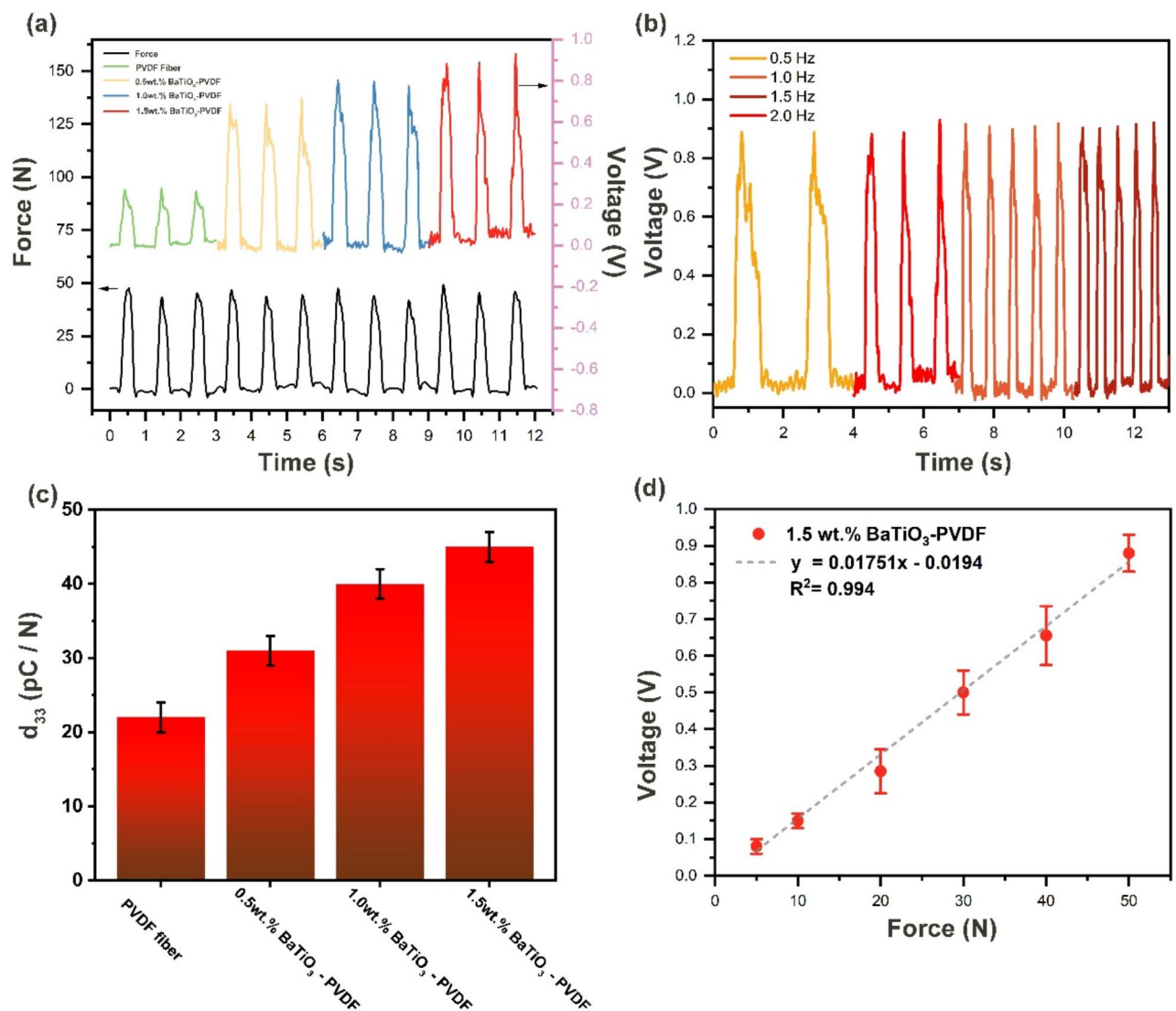
Fig. 5. **a**) V_{OC} response of BT/PVDF device employing 50 N load, (**b**) Isc response of the BT/PVDF device employing 50 N load. (**c**) d33 value of PVDF fiber with different BT content (0, 0.5, 1.0, 1.5 wt%) on the V_{OC} response of 1.5 wt% of BT/PVDF under 50 N load, (**d**) Effect of applying load (5 to 50 N) on the V_{OC} response of 1.5 wt% of BT/PVDF.

Data availability

Data is provided within the manuscript or supplementary information files.

References

1. Alhasssan, Z. A. et al. Polyvinylidene difluoride piezoelectric electrospun nanofibers: review in synthesis, fabrication, characterizations, and applications. *J. Nanomater.* 8164185 (2018). (2018)(1).
2. Wang, B. et al. Ultrasensitive cellular fluorocarbon piezoelectret pressure sensor for self-powered human physiological monitoring. *Nano Energy.* **32**, 42–49 (2017).
3. Deng, W. et al. Cowpea-structured PVDF/ZnO nanofibers based flexible self-powered piezoelectric bending motion sensor towards remote control of gestures. *Nano Energy.* **55**, 516–525 (2019).
4. Zeng, W. et al. Gradient CNT/PVDF piezoelectric composite with enhanced force-electric coupling for soccer training. *Nano Res.* **16**, 11312–11319 (2023).
5. Saxena, P. et al. A comprehensive review on fundamental properties and applications of poly(vinylidene fluoride)(PVDF). *Adv. Compos. Hybrid. Ma.* **4**, 8–26 (2021).
6. Mai, M. et al. Ferroelectric polymer thin films for organic electronics. *J. Nanomater.* **16** (1), 812538 (2015).
7. Mokhtari, F. et al. Recent advances of polymer-based piezoelectric composites for biomedical applications. *J. Mech. Behav. Biomed.* **122**, 104669 (2021).
8. Cauda, V. et al. Nanostructured piezoelectric polymers. *J. Appl. Polym. Sci.* **132** (13), 41667 (2015).

9. Won, S. S. et al. Lead-Free Bi0.5(Na$_{0.78}$K$_{0.22}$)TiO$_3$ nanoparticle Filler–Elastomeric composite films for Paper-Based flexible power generators. *Adv. Electron. Mater.* **6** (2), 1900950 (2020).
10. Baek, C. M. et al. Enhancement of power generation in hybrid Thermo-Magneto-Piezoelectric-Pyroelectric energy generator with piezoelectric polymer. *J. Korean Inst. Electr. Electron. Mater. Eng.* **36** (6), 620–626 (2023).
11. Sultana, A. et al. Methylammonium lead iodide incorporated Poly (vinylidene fluoride) nanofibers for flexible Piezoelectric–Pyroelectric nanogenerator. *Acs Appl. Mater. Inter.* **11** (30), 27279–27287 (2019).
12. Kalani, S. et al. Flexible electrospun PVDF–BaTiO$_3$ hybrid structure pressure sensor with enhanced efficiency. *RSC Adv.* **10** (58), 35090–35098 (2020).
13. Sappati, K. K. et al. Piezoelectric polymer and paper substrates: a review. *Sensors* **18** (11), 3605 (2018).
14. Saleem, S. et al. Modification in structural, optical, morphological, and electrical properties of zinc oxide (ZnO) nanoparticles (NPs) by metal (Ni, Co) dopants for electronic device applications. *Arab. J. Chem.* **15** (1), 103518 (2022).
15. Tang, H. et al. Nanocomposites with increased energy density through high aspect ratio PZT nanowires. *Nanotechnology* **22** (1), 015702 (2010).
16. Niu, Y. et al. Enhanced dielectric performance of BaTiO$_3$/PVDF composites prepared by modified process for energy storage applications. *IEEE T Ultrason. Ferr.* **62** (1), 108–115 (2015).
17. Shi, K. et al. Interface induced performance enhancement in flexible BaTiO$_3$/PVDF-TrFE based piezoelectric nanogenerators. *Nano Energy.* **80**, 105515 (2021).
18. Li, J. et al. Highly sensitive, flexible and wearable piezoelectric motion sensor based on PT promoted β-phase PVDF. *Sens. Actuat A-Phys.* **337**, 113415 (2022).
19. Shi, K. et al. Cellulose/BaTiO$_3$ aerogel paper based flexible piezoelectric nanogenerators and the electric coupling with triboelectricity. *Nano Energy.* **57**, 450–458 (2019).
20. Guo, H. et al. Organic phosphonic acid-modified BaTiO$_3$/P(VDF-TrFE) composite with high output in both voltage and power for flexible piezoelectric nanogenerators. *Mater. Today Energy.* **17**, 100489 (2020).
21. Yao, Z. et al. Homogeneous/inhomogeneous-structured dielectrics and their energy-storage performances. *Adv. Mater.* **29** (20), 1601727 (2017).
22. González-Benito, J. et al. PVDF based nanocomposites produced by solution blow spinning, structure and morphology induced by the presence of MWCNT and their consequences on some properties. *Colloid Polym. Sci.* **297**, 1105–1118 (2019).
23. Hernández, N. et al. Electrospun polyvinylidene fluoride nanofibers by bubble electrospinning technique. *Mater. Lett.* **167**, 34–37 (2016).
24. Röcker, T. et al. Electrospinning of poly-L-lactide nanofibers on liquid reservoir collectors. *e-Polymers* **8** (1), 111 (2008).
25. Kong, T. H. et al. Churros-like polyvinylidene fluoride nanofibers for enhancing output performance of triboelectric nanogenerators. *ACS Appl. Mater. Interfaces.* **12** (15), 17824–17832 (2020).
26. Zhang, X. et al. Improving dielectric properties of BaTiO$_3$/poly (vinylidene fluoride) composites by employing core-shell structured BaTiO$_3$@Poly(methylmethacrylate) and BaTiO$_3$@Poly (trifluoroethyl methacrylate) nanoparticles. *Appl. Surf. Sci.* **403**, 71–79 (2017).
27. Jung, J. T. et al. Understanding the non-solvent induced phase separation (NIPS) effect during the fabrication of microporous PVDF membranes via thermally induced phase separation (TIPS). *J. Membrane Sci.* **514**, 250–263 (2016).
28. Liu, F. et al. Progress in the production and modification of PVDF membranes. *J. Membrane Sci.* **375** (1), 1–27 (2011).
29. Li, S. et al. Electrospinning of circumferentially aligned polymer nanofibers floating on rotating water collector. *J. Appl. Polym. Sci.* **137** (22), 48759 (2020).
30. Chronakis, I. S. Novel nanocomposites and nanoceramics based on polymer nanofibers using electrospinning process-A review. *J. Mater. Process. Tech.* **167** (2–3), 283–293 (2005).
31. Yadav, S. K. et al. Enhanced mechanical and dielectric properties of poly(vinylidene fluoride)/polyurethane/multi-walled carbon nanotube nanocomposites. *Fiber Polym.* **10** (6), 756–760 (2009).
32. Cai, X. et al. A critical analysis of the A, B and γ phases in Poly (vinylidene fluoride) using FTIR. *RSC Adv.* **7** (25), 15382–15389 (2017).
33. Martins, P. et al. Electroactive phases of Poly (vinylidene fluoride): determination, processing and applications. *Prog Polym. Sci.* **39** (4), 683–706 (2014).
34. Athira, B. et al. High-performance flexible piezoelectric nanogenerator based on electrospun PVDF-BaTiO$_3$ nanofibers for self-powered vibration sensing applications. *ACS Appl. Mater. Interfaces.* **14** (39), 44239–44250 (2022).
35. Nguyen, M. D. et al. Large piezoelectric strain with ultra-low strain hysteresis in highly c-axis oriented Pb (Zr0.52Ti0.48)O3 films with columnar growth on amorphous glass substrates. *Sci. Rep.* **7** (1), 12915 (2017).
36. Wang, Z. L. The new field of nanopiezotronics. *Mater. Today.* **10** (5), 20–28 (2007).
37. Bellaiche, L. Intrinsic piezoelectric response in perovskite alloys: PMN-PT versus PZT. *Phys. Rev. Lett.* **83** (7), 1347–1350 (1999).
38. Fu, H. et al. Polarization rotation mechanism for ultrahigh electromechanical response in single-crystal piezoelectrics. *Nature* **403** (6767), 281–283 (2000).
39. Jiang, J. et al. Flexible piezoelectric pressure tactile sensor based on electrospun BaTiO3/poly (vinylidene fluoride) nanocomposite membrane. *ACS Appl. Mater. Interfaces.* **12** (30), 33989–33998 (2020).
40. Shi, K. et al. Synergistic effect of graphene nanosheet and BaTiO$_3$ nanoparticles on performance enhancement of electrospun PVDF nanofiber mat for flexible piezoelectric nanogenerators. *Nano Energy.* **52**, 153–162 (2018).

Acknowledgements

Author contributions

X.L. and Y.F. contributed equally to the conceptualization and design of the study. X.L. and G.P. performed the experiments and collected the data. X.L., X. L. and G.P. conducted the data analysis and interpretation. Y.F. and G.P. provided critical revisions and supervised the project. X.L., M.Z. and X.Z. wrote the manuscript, with input from all authors. All authors reviewed and approved the final version of the manuscript.

Declarations

Competing interests

The authors declare no competing interests.

Additional information

Supplementary Information The online version contains supplementary material available at https://doi.org/10.1038/s41598-025-96516-3.

Correspondence and requests for materials should be addressed to X.-W.L., P.G. or Y.F.

Reprints and permissions information is available at www.nature.com/reprints.

Publisher's note Springer Nature remains neutral with regard to jurisdictional claims in published maps and institutional affiliations.